Austin Journal of Biosensors & Bioelectronics

Open Access

Austin Publishing Group

Review Article

A High Resolution PDMS Based Elastography Imaging

Jong-Ha Lee*
Department of Biomedical Engineering, Keimyung University, South Korea

***Corresponding author:** Jong-Ha Lee, Department of Biomedical Engineering, Keimyung University, School of Medicine, South Korea

Received: November 21, 2016; **Accepted:** March 06, 2017; **Published:** April 03, 2017

Abstract

In this paper, a newly designed, high-resolution elasticity-imaging sensor using a total internal reflection of light is experimentally evaluated. The tactile sensor we propose is comprised of an elastic optical waveguide unit, a high resolution CCD camera unit, and an LED light source. The sensing element is formed on Polydimethylsiloxane (PDMS) and is illuminated along its four edges by LED light sources. The sensor operates on the principle of total internal reflection within an optical waveguide. To increase the sensitivity of sensing, an optical waveguide consisting of three different densities of PDMS with different elastic modulus was fabricated. From the experiments, the proposed sensor can differentiate the elasticity of the inclusion in tissue phantom through computational method.

Keywords: Elasticity tactile sensor; Elastography imaging; PDMS

Introduction

This paper describes an optical elasticity tactile sensor capable of sensing force and force position.

Diagnosing early formation of tumors or lumps, particularly those caused by cancer, has been a problem. It has been attempted to be solved using various techniques, such as computer tomography, ultrasonic imaging, nuclear magnetic resonance imaging, x-rays and so on. Each of these techniques has limitations, including the application of radiation to the body, which may be harmful to the body being tested. In breast cancer case, palpation plays a primary role in detecting tumors or lumps through breast self examination or annual clinical breast examination [1,2]. The problem with this method is that it is difficult to accurately verbalize and record tactile sensations. A variety of methods have been proposed for measuring the characteristics of tissue. One approach attempts to determine the relative stiffness or elasticity of tissue by applying ultrasonic imaging techniques while vibrating the tissue at low frequencies [3-5]. The tactile sensor we propose comprises anelastic optical waveguide unit, a high resolution CCD camera unit, a LED light source unit, and a laptop computer. The optical waveguide was formed on Poly Dimethylsiloxane (PDMS) and it is illuminated along its four edges by a LED light source. The tactile sensor operates on the principle of total internal reflection within an optical waveguide [6]. The light directed into the waveguide remains within it due to the total internal reflection generated, since the waveguide is surrounded by air having a lower refractive index than the waveguide. When an object adheres to the waveguide and compresses, the contact area of the waveguide deforms and causes the light to scatter. The normal force was detected from the integrated gray scale values of bright pixels emitted from the deformed area of the optical waveguide. The light from the deformed area is called frustrated total internal reflection lights. We analyze the physical basis for elasticity tactile imaging by measuring stress-strain patterns that result from frustrated total internal reflection lights pressed against objects [7]. Active contours or snakes are used to extract the optimal boundary of detected region. Laplacian smoothing splines are then used to estimate the displacement of points between the optimal boundaries [8]. The strain experienced throughout the object is then estimated using a non-rigid point matching algorithm. Temporal and spatial changes in the stress-strain pattern allow detection of external or internal structures with different elastic properties and assessment of geometrical and mechanical parameters of these structures.

The method will be finally implemented in the Tactile Elasticityimager (TEI) for breast tumor detection, a compact device consisting of a hand held probe equipped with an opticaltactile sensor. Palpation plays a primary role in detecting lumps through breast self examination or annual clinical breast examination. The problem with this method is that it is difficult to accurately verbalize and record tactile sensations. A method for accurately recording tactile sensations from physical exams would improve the ability to detect changes in lumps across time. Our goal is to develop a simple and easy to use system that can document the properties of palpable lumps in soft tissue. For this, the influence of some hidden anatomical features, such as lumps, on the stress distribution at the touching surface is studied through phantom test. Figure 1 shows the example of a breast self examination method and a tactile elasticity imaging method. By using a tactile imager, we can quantify the tactile sensation of hidden features. The tactile sensation would be more sensitive than what we are feeling it by hand.

Since the main motivation for creating tactile imaging and other elasticity imaging is to use elasticity data to differentiate normal and diseased tissue, the strain distribution for elasticity quantification based on the non-rigid point matching method is proposed. The stress and strain distribution map allows calculation of size, shape and consistency/hardness of detected lesions. We believe that tactile imaging will provide a solution to the problem of documenting the

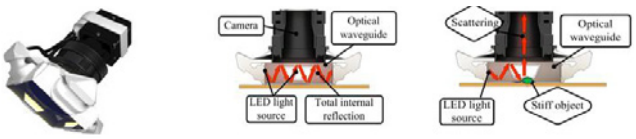

Figure 1: Schematic of the Optical Tactile Sensor.

Citation: Jong-Ha Lee. A High Resolution PDMS Based Elastography Imaging. Austin J Biosens & Bioelectron. 2017; 3(1): 1025.

results of physical examination. It will provide more accurate and repeatable estimates of lump size than the currently available widely used methods for breast examination specifically, clinical breast examination, ultrasound and mammography.

The tactile imaging system

System description and design: The schematic view shown in Figure 1 demonstrates the structure of the present sensor. The system uses a computer for data acquisition and analysis and a scan head that incorporates an elastic optical waveguide unit and aCMOS camera unit. Four LEDs light source unit are attached to the glass plate and illuminates an optical waveguide. Following section describes each unit in detail.

Elastic optical waveguide

The elastic optical waveguide is a main sensing probe of the device. The elastic optical waveguide is composed of Poly (dimethylsiloxane) (PDMS) [$Si(CH_3)_2$]. PDMS is the most important and the most useful high performance silicone elastomer. In the device, the optical waveguide requirestransparent and PDMS meets this requirement. One of Hydroxyl-terminated PDMS, RTV6100is purchased froma silicone distributor (R.S. Hughes, Baltimore, MD). The PDMSis produced by pouring viscous fluid silicone and catalyst into one mold. Here viscous fluid silicone is vinylstopped phenylmethypolyer and catalyst is a mixture of components including methylhydrogenpolysiloxane, dimethyl, methyvinyl siloxane and dimethylvinyl terminated. The viscous fluid silicone hardened by a catalyst and the hardness is depending on the ratio of silicone and catalyst. After mixing in a mold, it was cured for almost 1 day at room temperature. The final dimensions of the waveguide in the design are 21mm × 21mm × 20mm. Since the precision of the tactile sensor depends on the quality of the PDMS, optimal working conditions is necessary [9]. The refractive index of PDMS is an important optical parameter since it exhibits the optical properties of tactile sensor [10]. The refractive index of PDMS is changing depending on the mixture ratio of silicone and catalyst. Its values are often required to interpret various types of spectroscopic data. In this paper, we use quick measurements of refractive indices using simple technique as follows.

A glass plate such as a microscope slide is placed in a shallow tray on a table. The glass must be perfectly horizontal. A He-Ne laser is reflected off the surface of the glass to produce a spot of light, N on a vertical wall.

Without moving glass plate, place a PDMS on the glass. We should then get two spots appearing on the wall: one from the reflection on the surface of the liquid (M_2) and one from the beam which refracts through the liquid and reflects from the glass (M_1). The incident angle Θ of the laser beam is easily found by measuring OD and ON:

$$\tan\Theta = OD/ON. \quad (1)$$

Assuming that air has a refractive index n_2 of 1, PDMS has a relative refractive index n_1 given by

$$n_1 = \frac{\sin[\tan^{-1}(OD/ON)]}{\sin\{\tan^{-1}[M_2M_1/NM_2)OD/ON]\}}. \quad (2)$$

It should be noted that there is a minimum necessary thickness of the PDMS for the point M_1 and M_2 to be solved. The experiment can be repeated for different angles of incidence and for different thicknesses of PDMS. Theschematic of this concept is shown in Figure 3. Four

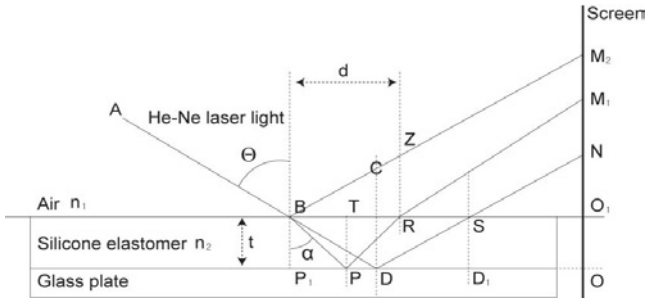

Figure 2: Refractive Index Measurement.

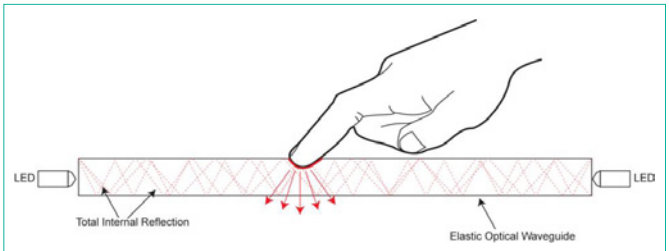

Figure 3: Tactile sensation concept using total internal reflection.

measurements of the refractive index of PDMS mixed at a ratio of silicone: catalyst = 3:1 gave an average value of 1.41±0.02 [11].

It is necessary to determine an appropriate size and shape of an optical waveguide. One might argue that a finger sized head with a comparable radius of curvature would be appropriate, because it would allow the examiner to press deeply into the tissue with little input force. However, this poses a problem because the stress field across the surface of the indenter when they are pressed into an object. These variations would make the appearance of a lump vary greatly. In the current design, the flat waveguide is necessary to produce uniform pressure distribution [12].

CMOS camera: The high performance CMOS camera is placed below an optical waveguide. The clear glass is placed between CMOS camera and an optical waveguide to sustain an elastic optical waveguide without losing camera resolution. The digital imager is a mono-cooled Complementary Metal–Oxide–Semiconductor (CMOS) The maximumresolution is 1392 (H) × 1042 (V).

Internal light source: The internal light source is a micro LED (Unique-Leds, Newalla, OK) with a diameter of 1.8 mm. There are 4 LEDs to provide enough illumination for the optical waveguide.

Sensing principle: The tactile sensor operates on the principle of total internal reflection. Beams of light emitted from the light source to the edge of the optical waveguide, are totally enclosed and reflected inside the optical waveguide. The tactile sensor uses the deformable properties of the fingerpad as part of the transduction process. The light from a light source is injected into a waveguide from its edge. The innermost region of a waveguide carried the light, while preventing the light from leaking out of the silicone by reflecting the light within the boundaries of the silicone. When an object touch to the optical waveguide and compress, the deformed area causes the light to scatter, and are observed from the rear side of the transparent mirror. The concept is shown in Figure 3.

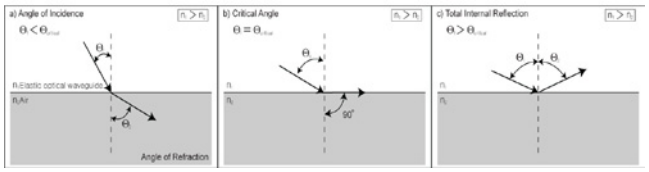

Figure 4: Equations for Snell's Law.

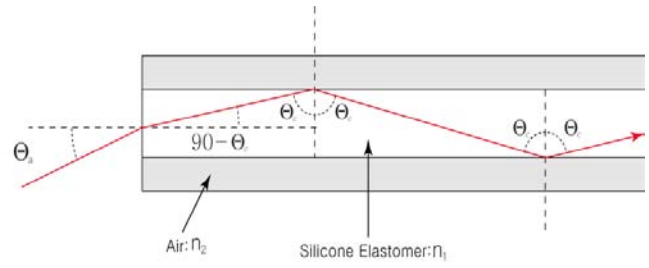

Figure 5: Criticalangle cone andacceptance angle in total internal reflection.

Snell's Law explains total internal reflection. It states that the angle at which light reflects as it passes from one material to another depends on the refractive indices of the two materials– in this case, the elastic optical waveguide and the air.

Figure 4 illustrates the equations for Snell's Law. From the Figure 5a to 5c, the incidence angle has increased to a value greater than the critical angle. Once the incidence angle is greater than the critical angle, 100 % of the light reflects at the interface region. The principle of total internal reflection governs the operation of tactile sensor. This occurs because light travels at different speeds in different materials. The index of refraction is the ratio of the velocity of light in a vacuum *c* to its velocity in a specific medium *v* as *n=c/v*. Light bends or refracts as it passes from a medium of one refractive index to a medium with a different refractive index. Shell's law determines the amount of light that bends as follows.

$$n_1 \sin\Theta_1 = n_2 \sin\Theta_2 . \quad (3)$$

Increasing the angle of incidence over the critical angle results in total internal reflection. The critical angle is calculated as below.

$$\Theta_c = \sin^{-1}(n_2 / n_1). \quad (4)$$

An imaginary cone of acceptance with an angle Θ_a, determined by the critical angle, relates to a parameter called the Numerical Aperture (NA) of the silicone elastomer. NA describes the light gathering capability of silicone elastomer. When a light ray is incident from a medium of refractive index *n* to the silicone elastomer of index n_1, Snell's law at medium silicone elastomer interface gives

$$n_2 \sin\Theta_a = n_1 \sin\Theta_r . \quad (5)$$

From the Figure 5 and using trigonometry, we get $\sin\Theta_r = \sin(90-\Theta_c) = \cos\Theta_c$ where $\Theta_c = \sin^{-1}(n_2 / n_1)$ the critical angle for total internal reflection is. After substituting we get:

$$(n_2 / n_1)\sin\Theta_a = \cos\Theta_c \quad (6)$$

By squaring both sides

$$(n_2^2 / n_1^2)\sin^2\Theta_a = \cos^2\Theta_c = 1-\sin^2\Theta_c = 1-n_2^2/n_1^2 \quad (7)$$

Thus the numerical aperture NA is

$$NA = n_2 \sin\Theta_a = \sqrt{n_1^2 - n_2^2}, \quad (8)$$

and the cone of acceptance angle is

$$\Theta_a = 1/n_2(\sin^{-1}(\sqrt{n_1^2 - n_2^2})). \quad (9)$$

Here is the example. The elastic optical waveguide consists of PDMS and its refractive index n_1 measured from II-A-1) is approximately 1.41. The outside of waveguide is an air and the refractive index of air n_2 is 1. Because the silicone elastomer has a higher index of refraction than the air ($n_1 > n_2$), it allows total internal reflection to occur. In this case, the critical angle is $\Theta_c = \sin^{-1}(1/1.41) = 45.17^o$ and the numerical aperture to be $NA = \sqrt{(1.41^2 - 1^2)} = 0.994$. Finally, the imaginary cone of acceptance angle Θ_a is $\Theta_a = \sin^{-1}(0.994) = 83.72$.

Characteristics of the sensor

Calibration: Since PDMS is produced in the University Laboratory environment, purity is an issue. To minimize the amount of air entrapment, vacuum deaeration can be used to remove entrapped air from the uncured mixture. However in this paper, instead of using vacuum deaeration, the optical calibration method is used.

The tactile image intensity at spatial coordinate *(x,y)* can be modeled as,

$$I(x,y) = L(x,y)S(x,y)R(x,y) + O(x,y), \quad (10)$$

where *x* = 1,2,…,1392 and *y* = 1,2,…,1042 and it depends on the camera resolution. *L(x,y)* refers to the illumination, *S(x,y)* refers to the sensor response, *R(x,y)* refers to the reflectance of the viewed surface, and *O(x,y)* is the offset due to the stray of the light. To compensate the unknown sensor offsets and gains, Spectralon diffuse reflectance standards SRS-99 for an approximately 99 % reflectance and SRS-02 for an approximately 2 % reflectance are used (Labsphere, Sutton, NH). These standards used in the calibration are directly traceable to the US National Institute of Standards and Technology (NIST). For the image reflectance of SRS-99 spectralon, we placed SRS-99 in front of PDMS and obtained the image. The image intensity of SRS-99 spectralon is as follows:

$$I_{SRS-99}(x,y) = L(x,y)S(x,y)R_{SRS-99}(x,y) + O(x,y). \quad (11)$$

And for the image intensity of SRS-02 spectralon, we have

$$I_{SRS-02}(x,y) = L(x,y)S(x,y)R_{SRS-02}(x,y) + O(x,y), \quad (12)$$

where $R_{SRS-99}(x,y)$ and $R_{SRS-02}(x,y)$ are reflectance functions for these two images and theoretically independent of a point *(x,y)* because the spectralon surface has the same reflectance property for all image pixels. By using the equations for $I_{SRS-99}(x,y)$ and $R_{SRS-02}(x,y)$, we can derive.

$$L(x,y)S(x,y) = \frac{I_{SRS-02}(x,y) - I_{SRS-99}(x,y)}{R_{SRS-02}(x,y) - R_{SRS-99}(x,y)}. \quad (13)$$

20 different spectralon images were obtained and averaged to estimate $I_{SRS-99}(x,y)$ and $R_{SRS-02}(x,y)$. With this estimates, the final reflectance is given as below:

$$R(x,y) = \frac{(I(x,y) - I_{SRS-99}(x,y))R_{SRS-02}(x,y)}{I_{SRS-02}(x,y) - I_{SRS-99}(x,y)} + \frac{(I_{SRS-02}(x,y) - I(x,y))R_{SRS-99}(x,y)}{I_{SRS-02}(x,y) - I_{SRS-99}(x,y)}. \quad (14)$$

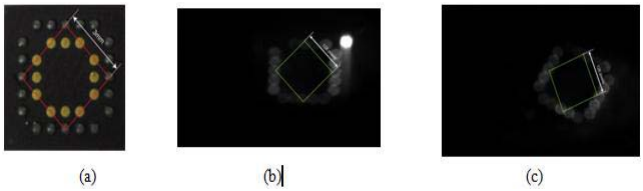

Figure 6: (a) Picture of the 32-lead chip ball grid array. (b) Tactile image of the ball grid array with 10 degree turned right. (c) Tactile image of the ball grid array with 30 degree turned right. The images on two slightly tilted angles show the measurement performance.

Figure 7: (a) Picture of the protoboard. (b) Tactile images of the protoboard.

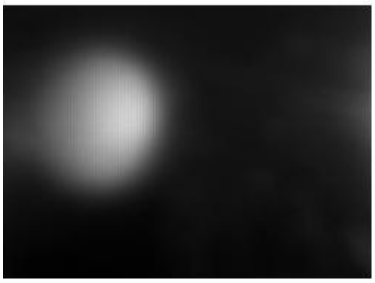

Figure 8: Tactile image under 1 Nloading.

Resolution

This section shows the achieved tactile images of two references using the developed tactile sensor. One of the references is a 32-lead chip ball grid array, as shown in Figure 6a. The chip has several conducting balls running parallel on each direction on the same flat plane. The spacing of the balls is 1.00 mm. The peak of the ball is 0.25 mm. As shown in Figure 6b and 6c, the tactile images of the array in two different angles show the uniformity and repeatabilityof the sensing area. The 3 mm spacing between middle balls in each side is used as the reference length and the corresponding pixel length in the tactile image was 126±10 pixels. The sensing area is at least 400 mm^2 and a scale factor is 0.006797±0.0005 mm per pixel. If we assume that one pixel is one pressure sensor, the pressure sensor is placed every 6.8×10^{-3} mm. The density of pressure sensors of at least 5970 are placed in a sensing area 20mm×20 mm.

The image represents the measurement accuracy of two orthogonal directions of the sensing area. An additional calibration result of the sensor is done using a protoboard. A protoboard consists of a perforated block of plastic shown in Figure 7a. A individual block size is 2.54mm×2.54 mm. Figure 7b shows the tactile image of a protoboard. The tactile image shows the measurement performance of two orthogonal directions of the sensing area. All reference tactile images are obtained under 2 N normal force. Two reference results demonstrated the consistency and high performance of the developed tactile sensor.

Data processing and imaging algorithms

Noise Reduction

3D Reconstruction: For constructing three-dimensional model, we use a reflectance *R(x,y)* and relates to the surface normal *N(x,y)*. To derive the surface normal of 2D tactile image, the radiosity at a point *(x,y)* on the surface of the object is given by

$$B(x,y) = \rho(x,y)N(x,y)\cdot L, \quad (15)$$

where $\rho(x,y)$ is the surface albedo, *N(x,y)* is the surface normal, and *L* is the light source vector. Assuming that the reflectance is linear with respect to the surface radiosity *B(x,y)*.

Then the reflectance value of each pixel can be written as

$$R(x,y) = kB(x,y) = k\rho(x,y)N(x,y)\cdot L = g(x,y)\cdot V, \quad (16)$$

where *k* is the constant and *V = k.L*. If we assume that the sensor surface is the Lambert surface with albedo 1 and *V* is a vector as $(0,0,1)^T$, i.e., along the x, y, and z-axis, then *N(x,y)* can be found as

$$N(x,y) = \frac{R(x,y)}{\|R(x,y)\|_2}. \quad (17)$$

Once the field of normal is built, we can easily recover the z-coordinate for each point in the mesh. If we assume that the value of the unit normal at some point *(x,y)* is *(a(x,y), b(x,y), c(x,y))* and *Z(x,y)* is the function of the surface, it is easy to see that $\frac{\partial z}{\partial x} = \frac{-a(x,y)}{c(x,y)}$ and $\frac{\partial z}{\partial y} = \frac{-b(x,y)}{c(x,y)}$. If we assume that the z-value at some reference point P_0 is 0, the z-value at any other point P_d will be a linear integral of $(\frac{\partial z}{\partial x}, \frac{\partial z}{\partial y})$ along the path from P_0 to P_d.

Elasticity calculation

An elastic modulus or Young's modulus is the mathematical description of an object to be deformed elastically when a force is applied to it. The elastic modulus of an object is defined as the slope of its stress-strain curve in the elastic deformation region. In this section, elasticity calculation method is provided.

Normal force detection

To find the applied normal force value from the tactile image, the relationship between the contact force F_Z and the calibrated gray scale light spot intensity *R(x,y)* is evaluated. Since the camera is 8 bit digital imager, each value of *R(x,y)* is quantified by a gray scale level and has a minimum of 0 and has a maximum value of 2^8=256. In this experiment, a sharp tip attached to the force/torque gauge (Mecmesin, West Sussex, UK) is used to contact the tactile sensor. The resulting light spot is captured by the tactile sensor and the corresponding contact force is measured by the force gauge. A pixel value is correspondingto the pressure value, and total pixel values measured to determine pressure characteristics. Figure 8 shows one example of tactile images under 1 N loading.The original image is enhanced by the linear filter.

Since the gray scale light spot *R(x,y)* of the tactile image is proportional to the contact pressure *S(x,y)* caused by the contact between optical waveguide and an object, it can be expressed as follow:

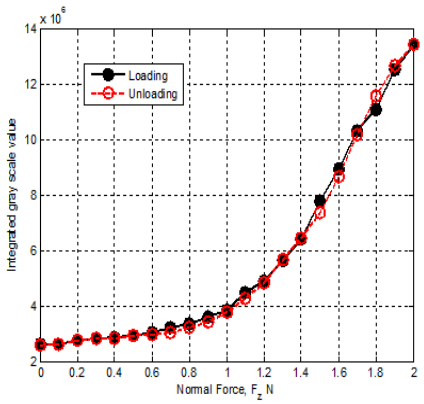

Figure 9: The relationship between normal force and integrated gray scale value.

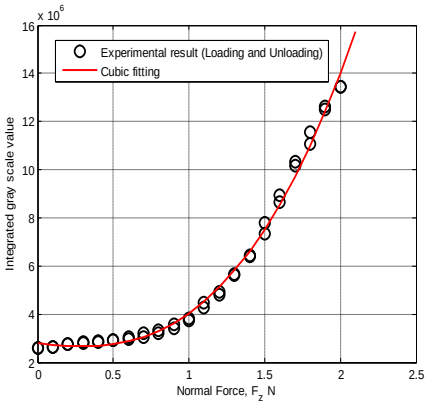

Figure 10: Cubic fitting of loading unloading data.

$$p(x,y) = CR(x,y), \tag{18}$$

where C is the conversion factor. If S is designated as the contact area of a silicone and an object and the vertical force F_Z is obtained by integrating the pressure over the contact area as follows:

$$F_z = \int_S p(x,y)dS. \tag{19}$$

If we substituted, then, the vertical force is $F_z = \int_S p(x,y)dS = \int_S Cg(x,y)dS \equiv CG$ where the integration of $g(x,y)$ over the contact area S is denoted as G.

To validate the normal force detection, after starting from the initial load of 0 mN, the normal force is increased in a stepwise manner. When the applied force reaches the maximum force, in this experiment, 2 N, the appliednormal force decreases in a stepwise fashion until it returns to 0 N. Figure 9. shows the relationship between the integrated gray scale value and the applied normal force.

The fitting curve was achieved using a cubic fitting method as shown in Figure 10. The curve approximately represents the monotone increasing relationship between the contact force F_Z and the integrated gray scale value G of the tactile image as follows:

$$G(F_z) = 2.799\times10^6 - 0.883F_z + 1.003F_z^2 + 1.121\times10^6 F_z^3. \tag{11}$$

Modulus estimation

In this section, a modulus estimation method is presented. First

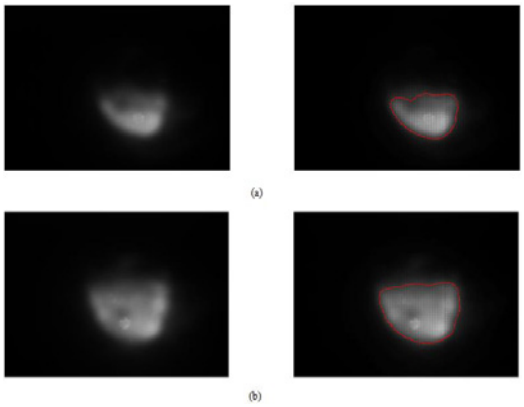

Figure 11: An optimal boundary of a 10mm × 10mm Zerdinetactile images. The force applied to Zerdine in (b) is bigger than the force applied to Zerdinein (a).

a scheme for obtaining strain maps for a set of tactile images is described.

The first stage of the tactile image analysis involves the extraction of the contours of the object from each image. This process was done using active contours or snakes. Snakes consist of a set of points $V(s)=(x(s),y(s))$, $0<s<1$, which are attracted towards a feature of interest within an image through minimizing the energy term

$$E_{snake} = E_{internal} + E_{image} + E_{external}. \tag{12}$$

The internal energy describes the smoothness of the points, and is defined as

$$E_{internal} = \frac{1}{2}\int_0^1 \alpha \left\|\frac{dv(s)}{ds}\right\| + \beta \left\|\frac{d^2v(s)}{ds^2}\right\| ds. \tag{13}$$

where the coefficients α and β control the amount of stretching and bending available.

The image energy is a function of the image intensity I and its derivative with respect to the image axis, i_x and i_y:

$$E_{image} = \int_0^1 \alpha I_{v(s)} + \beta\left(\frac{dI}{dx}\right)_{v(s)} + \gamma\left(\frac{dI}{dy}\right)_{v(s)} ds. \tag{14}$$

where the coefficients α, β and γ control the importance of the different intensity measure. Through minimizing the image energy the points are attracted to the darker regions of an image and the regions where there is a large contrast in image intensity, that is borders between light and dark regions. The area inside a snake is an optimal area.

Due to the nature of nonlinear optimization, snakes may often be attracted to local minima or undesired features of interest. This is overcome by introducing a term labeled the external energy. In this case, a user observes the snake moving towards the desired feature of interest, and stops the procedure when the snake appears to be moving in the wrong direction. The user then applies a point force which adjusts the snake points by an arbitrary amount back towards the desired feature of interest. In this way the snake is moved away from local minima and back towards the feature of interest within an image.

We idealize the behavior of test material as nearly elastic and isotropic.We can draw a circle with same optimal area of tactile iamge. Then the strain can be express as a changed radius of an optimal area

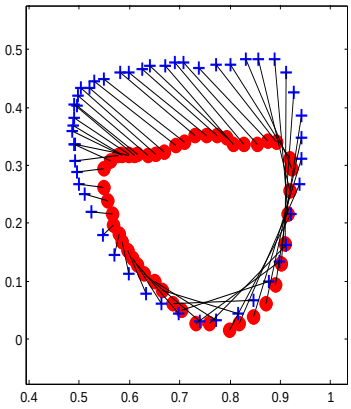

Figure 12: The displacement filed estimated by non-rigid point matching algorithm.

between two images. Let the optimal area as A then the strain is

$$strain = |\frac{r_1 - r_2}{r_1}|, \quad (15)$$

where $r = \sqrt{A/\pi}$.

Figure 11 demonstrate the application of snakes within tactile images of Ball shape Zerdine material with 4000 Pa elastic modulus. Two tactile images are obtained under different forces. As we can see, the optimal boundary is located for each imagethroughout the set, and hence the displacement determined by considering the position of the lines at different times.

In Zerdine tactile images, the corresponding optimal area and radius offirst image is A_1=35.15mm^2 with r_1=4.383m and a second image is A_2=60.349mm^2 with r_2=3.345m. The strainbetween two images is 0.31. Once we found the normal force and strain, the elastic modulus calculation is pretty simple.

$$Elastic\ modulus = stress/strain \quad (16)$$

The relationship between integrated gray scale value and the corresponding normal force is already found in (4.3). We found that the corresponding normal force of the integrated gray scale value G_1=3404857 is 0.841 N and the normal force for G_2=5839379 is 1.34 N. Then the applied stress on Zerdine is $(1.34N\text{-}0.83N) / 400mm^2$. The final elastic modulus we obtained is approximately 4.11kPa. Compare to the original Zerdine elastic modulus 4kPa, the error is 2.85 %.

Generating a displacement surface using laplacian splines

If the test material undergoes much change in modulus with strain, the displacement surface can be constructed Laplacian spline function. Here we use thin plate spline which is the best known of Laplacian splines. A subsample of 50 points randomly selected from the optimal boundary is generated to estimate a displacement field. The displacement field is found using non rigid point matching algorithm. The result is shown in Figure 12.

The spline f can be generated from a subsample of 50 points randomly selected from the optimal boundary. The generation of strain maps from the displacement surfaces is a fairly simple procedure. The nonlinear Lagrangian strain tensor ε is defined as,

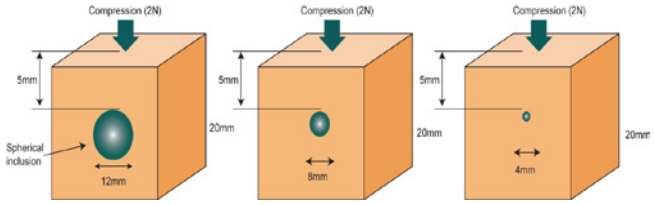

Figure 13: An example of the strain experienced as a function of the inclusion size. (a) Tissue sample with 12 mm inclusion. (b) Tissue sample with 8 mm inclusion. (c) Tissue sample with 4 mm inclusion.

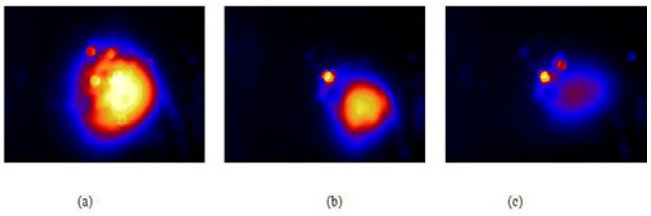

Figure 14: Tactile images from three different sizes of inclusions. (a) Tactile image with 12 mm inclusion. (b) Tactile image with 8 mm inclusion. (c) Tactile image with 4 mm inclusion. All images are obtained under 4 N compressions.

$$\varepsilon_{ij} = \frac{1}{2}\left(\frac{\partial f_i}{\partial x_j} + \frac{\partial f_j}{\partial x_i} + \sum_{k=1}^{2} \frac{\partial^2 f_k}{\partial x_i \partial x_j}\right). \quad (17)$$

where $i, j = 1,2$

Experimental Results

Measurement accuracy as a function of the inclusion size

Realistic breast tissue phantoms shown with embedded hard nodules have been prepared. This model was made of a Zerdine composite having Young's modulus of 4 kPa with an array of hard spherical inclusions embedded at different depth in the model. The phantom thickness measured 20 mm, inclusions were placed 5mm below the upper surface of the phantoms. The inclusion was ball made by *Play-Doh (Play-Doh*, Hasbro Ltd., Newport, UK). The size was 12mm, 8mm, 4mm. The tactile images are obtained under the same force 2N. Figure 13 shows the experimental concept.

Figure 14 shows the corresponding tactile images. The optimal boundary area of sensed tactile image becomes smaller as the corresponding inclusions getting smaller.

Because the light scatters on the contact area, the gray scale value of the contact image acquired by the CCD camera distributes as a bell shape, in which the gray scale intensity is the highest at the centroid and decrease with increasing distance from centroid of the deformed area. To compare the tactile image, the horizontal tactile data through centroid is obtained and the Gaussian fitting model is used to describe the shape of tactile data. From this curve, we get the following Gaussian function and from this equation we obtain pressure intensity distribution Figure 15.

$$P = ae^{-x^2/2\sigma^2} \quad (18)$$

The amplitude of each Gaussian function is a_1=234.23, a_2=137.06, and a_3=77.07. The variance is σ_1^2=99.96, σ_2^2=98.92, and σ_3^2=75.40. From this data, we can clearly see the difference between three data.

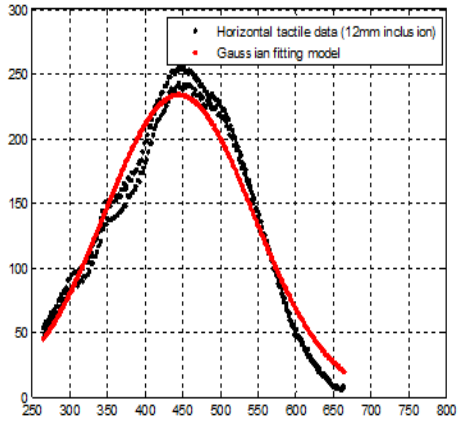

Figure 15: Horizontal tactile data and its Gaussian fitting model.

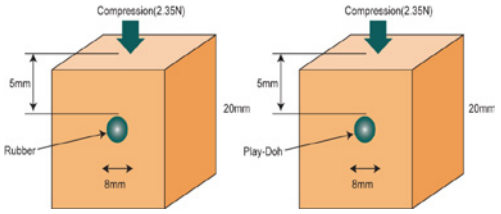

Figure 16: An example of the strain experienced as a function of the different inclusion. (a) Tissue sample with 8 mm rubber inclusion. (b) Tissue sample with 8 mm Play-Doh inclusion.

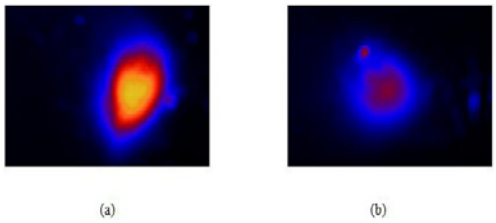

Figure 17: Tactile images from two different inclusions. (a) Tactile image of rubber. (b) Tactile image of *Play-Doh.*

Measurement accuracy as a function of the different inclusion

In this experiment, the phantoms had an inclusion with diameter 8mm of *Play-Doh* and rubber. Typically, the rubber has much higher elastic modulus than Play-Doh. Total phantom thickness was 20 mm, and the base material Young's modulus of 4 kPa.The inclusions were placed 5 mm below the upper surface of the phantoms. The tactile images are generated under 2.35 N. Figure 16 shows the experimental concept. The sensed tactile images that we obtained are shown in Figure 17.

Figure 18 represents a Gaussian fitting model. The rubber tactile data has a_1=175.20 with σ_1^2 =80.25 and the *Play-Doh* tactile data has a_1=81.62 with σ_1^2 =98.64.

Conclusion

In this paper, a newly designed, high-resolution elasticity-imaging sensor using a total internal reflection of light is experimentally evaluated. The tactile sensor we propose is comprised of an elastic optical waveguide unit, a high resolution CCD camera unit, and an LED light source. The sensing element is formed on Polydimethylsiloxane (PDMS) and is illuminated along its four edges by LED light sources. The sensor operates on the principle of total internal reflection within an optical waveguide. To increase the sensitivity of sensing, an optical waveguide consisting of three different densities of PDMS with different elastic modulus was fabricated. From the experiments, the proposed sensor can differentiate the elasticity of the inclusion in tissue phantom through computational method.

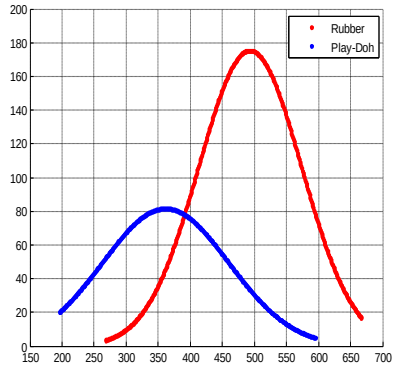

Figure 18: Three Gaussian fitting models depending on inclusion size.

Acknowledgement

The research was supported by the Ministry of Trade, Industry & Energy (MOTIE, Korea) under Industrial Technology Innovation Program, No. 10063553, (Self-directed portable safety kits and application based living environment service systemandthis work (Grants No. C0395986) was supported by Business for Cooperative R&D between Industry, Academy, and Research Institute funded Korea Small and Medium Business Administration in 2017.

References

1. Kamangar F, Dores GM, Anderson WF. Patterns of cancer incidence, mortality, and prevalence across five continents: definingpriorities to reduce cancer disparities in different geographic regions ofthe world. J Clin Oncol. 2006; 24: 2137-2150.
2. Jemal, Siegel R, Ward E, Hao Y, Xu J, Thun MJ. Cancer statistics. CA: A Cancer Journal for Clinicians. 2009; 59: 225-249.
3. Shojaku H, Seto H, Iwai H, Kitazawa S, Fukushima W, Saito K. Detection of incidental breast tumors by noncontrast spiral computedtomography of the chest. Radiat Med. 2008; 26: 362-367.
4. Fenster, Downey DB. 3-D ultrasound imaging: a review. IEEEEng Med Biol Mag. 1996; 15: 41-51.
5. Degani H, Gusis V, Weinstein D, Fields S, Strano S. Mapping pathophysiological features of breast tumors by MRI at high spatial resolution. Nat Med. 1997; 3: 780-782.
6. Gentle R. Mammobarography: a possible method of mass breast screening. J Biomed Eng. 1988; 10: 124-126.
7. Harberland N, Ebmeier K, Hliscs R, Grunewald J, Kalff R. Intraoperative CT in image-guided surgery of the spine. Journal of Medicamundi. 1999; 43: 24-32.
8. Gwinn R, Cleary K, Medlock M. Use of portable CT scanner during resection of subcortical supratentorial astocytomas of childhood. Journal of Pediatric Neurosurgery. 2000; 32: 37-43.
9. Gentle CR. Mammobarography: a possible method of mass breast screening. Journal of Biomedical Engineering. 1988; 10: 124-126.

10. Schulder, Carmel P. Intraoperative magnetic resonance imaging: impact on brain tumor surgery. Journal of Cancer Control. 2003; 10: 115-125.

11. Wolverson M, Houttuin E, Heiberg E, Sundaram M, Shields J. Comparison of computed tomography with high resolution real time ultrasound in the localization of the impalpable undescended testis. Journal of Radiology. 1983; 146: 133-136.

12. Kaufman L, Jacobson B, Bachman, Kaufman L. Intraoperative ultrasound facilitates surgery for early breast cancer. Journal of Annals of Surgical Oncology. 2007; 9: 988-993.

Austin J Biosens & Bioelectron - Volume 3 Issue 1 - 2017
ISSN : 2473-0629 | www.austinpublishinggroup.com

Citation: Jong-Ha Lee. A High Resolution PDMS Based Elastography Imaging. Austin J Biosens & Bioelectron. 2017; 3(1): 1025.